

The impacts of dark matter particle annihilation on recombination and the anisotropies of the cosmic microwave background

Le Zhang,^{1,2} Xuelei Chen,^{1,*} Yi-An Lei,³ and Zong-guo Si²

¹*National Astronomical Observatories, Chinese Academy of Sciences, Beijing, 100012, China*

²*Department of Physics, Shandong University, Jinan, 250100, China*

³*Department of Physics, Peking University, Beijing, 100871, China*

The recombination history of the Universe provides a useful tool for constraining the annihilation of dark matter particles. Even a small fraction of dark matter particles annihilated during the cosmic dark age can provide sufficient energy to affect the ionization state of the baryonic gas. Although this effect is too small for neutralinos, lighter dark matter particle candidates, e.g. with mass of 1-100 MeV, which was proposed recently to explain the observed excess of positrons in the Galactic Center, may generate observable differences in the cosmic microwave background (CMB) temperature and polarization anisotropies. The annihilations at the era of recombination affects mainly the CMB anisotropy at small angular scales (large ℓ), and is distinctively different from the effect of early reionization. We perform a multi-parameter analysis of the CMB data, including both the WMAP first year and three year data, and the ACBAR, Boomerang, CBI, and VSA data. Assuming that the observed excess of e^+e^- pairs in the galactic center region is produced by dark matter annihilation, and that a sizable fraction of the energy produced in the annihilation is deposited in the baryonic gas during recombination, we obtain a %95 dark matter mass limit of $M < 8\text{MeV}$ with the current data set.

I. INTRODUCTION

The presence of dark matter, and much of what we now know about it, were derived from creative analysis of astronomical observations. For example, from the abundance of the light elements, it has been deduced that the dark matter must be non-baryonic; and from the large scale structure of galaxies, the hot dark matter candidates such as massive neutrinos were excluded. Currently, various astronomical observations, from gravitational lensing to the composition of cosmic rays are being studied in searches of the dark matter [1].

The ionization history of the Universe provides us with a very useful tool to investigate the properties of dark matter. According to the Cold Dark Matter model with a cosmological constant (Λ CDM) model, which is now standard in cosmology, at redshifts of about 1000, the temperature of the radiation background photons was lowered sufficiently that the free electrons and protons could recombine to form neutral hydrogen atoms. As the number of free electrons decreased, the gas became transparent, and most of the radiation background photons scattered for the last time. This epoch of recombination marks the end of the hot Big Bang and the beginning of the so called cosmic dark age, and much information about the last scattering surface is preserved in the CMB anisotropies. The dark age lasted until the first stars formed by growth of primordial density fluctuations. Eventually, the light emitted by the galaxies reionized the Universe [2, 3].

However, the history of the Universe would be different, if the dark matter particles played a more *active*

role during the cosmic dark age. If the dark matter particles could decay or annihilate, extra energy would be injected into the baryonic gas. This could delay recombination, or make the Universe reionize earlier. These effects are observable with high precision CMB data. In 2003, the Wilkinson Microwave Anisotropy Probe (WMAP) team published the result of their first year observation [4, 5, 6, 7, 8, 9]. A strong correlation of the temperature and the E-like polarization anisotropy (TE) was observed at large angular scales (small ℓ) [7, 9]. Such correlation could be generated by the scattering of the CMB photons by free electrons after the reionization of the Universe [9, 10, 11, 12]. The best fit model requires reionization to happen at redshift 20, which is much earlier than predicted by the Λ CDM model [13, 14, 15, 16, 17]. A number of researchers has suggested that the decay of dark matter particle could make the reionization happen earlier, which helps to explain the WMAP result [18, 19, 20, 21, 22, 23, 24]. Alternatively, using the CMB data, one could constrain the decay property of the dark matter particle. As the energy corresponding to the rest mass of the dark matter particle is much higher than the ionization energy of the hydrogen atom, even if only a very small fraction of dark matter particles decayed, it could inject sufficient energy to the baryonic gas to alter the ionization history, and affect the CMB anisotropies. This can be used to exclude the short-lived decaying particles with life time comparable to the age of the Universe at the epoch of recombination [18].

In the present work, we consider the impact of dark matter annihilation on the recombination process. Many dark matter candidate particles could annihilate and produce γ -ray photons, energetic electrons and positrons, and hadronic particles which ionize the gas in the environs. For example, the annihilation processes of the supersymmetric dark matter candidate neutralino have

*Electronic address: xuelei@bao.ac.cn

been well studied [25]. For neutralinos, however, the annihilation rate is fairly small. Since the annihilation rate is proportional to the squared number density of the dark matter particle, lighter particles would produce stronger annihilation signals. Recently, a 511 keV emission line in the direction of the Galactic Center was observed by the SPI spectrometer on board of the INTEGRAL satellite [26]. This discovery indicates the presence of large amount of positrons in that region. It has been pointed out that if the dark matter particle is not neutralino but a light scalar particle with mass of 1–100 MeV and weak interaction cross sections [27, 28], then the annihilation rate would be high enough to produce these positrons. Other models which attempts to explain this with dark matter include the decay of dark matter particle [29] or the annihilation of relic heavy neutrino with long range interaction [30].

At the epoch of recombination ($z \sim 1000$), the annihilation rate could be even greater due to the higher densities, and then it might make an imprint on the recombination history. In Refs. [24, 31] this effect was illustrated with a few models. However, no concrete limit on dark matter annihilation has been obtained with the current CMB data. To obtain such a limit, one needs to calculate the CMB anisotropy with dark matter annihilation and compare it with the data. In doing so, it is of crucial importance to break the degeneracies among the many cosmological parameters, because all of these parameters affect the CMB angular power spectrum in different ways, and a change in the power spectrum caused by one parameter might be compensated by the combined variation of several other parameters.

In the present work, we break the degeneracies among the cosmological parameters by exploring the multi-dimensional parameter space with the Markov Chain Monte Carlo technique [32, 33, 34]. We modify the publicly available MCMC code COSMOMC [34, 35], which uses CAMB [36, 37] as its CMB driver, particularly the ionization evolution code RECFAST [38] embedded in it, to take into account the effect of energy injection due to dark matter annihilation. We also compare the MCMC result with the Fisher matrix estimate, to gain insights on how reliable is the latter method. We then use the Fisher matrix method to make forecasts on the potential of future experiments such as the Planck mission [39, 40].

In the first version of this paper, we used the first year WMAP data [4, 5, 6, 7, 8, 9], as well as the data obtained by the ACBAR [41], Boomerang [42], CBI [43], and VSA [44] experiments in our analysis. Shortly after its submission, the WMAP team released their three year observation data [45, 46, 47, 48, 49]. The error of the observation is reduced. Also, it is now believed that the large TE correlation at low ℓ observed in the first year is due to contamination by foreground. The current estimate of the reionization optical depth τ is much smaller. We have repeated our analysis with this new data set, and found that with the reduced errors in the three year data, the constraint on dark matter annihilation is much

stronger. The change on τ does not significantly affect our result, because as we shall discuss below, our constraint comes mainly from the epoch of recombination, not the epoch of reionization. In this second version, we retain some results obtained in the first version, but added new results obtained with the new data.

In the following, we describe our method of calculation in §II, and present our results in §III, with a synthesis of current constraint on MeV dark matter obtained with different methods. We summarize our results in §IV.

II. METHODS

The evolution of the ionization fraction and temperature of the baryonic gas is given by Eq. (15) and Eq. (23) of Ref. [18], which we reproduce here:

$$(1+z)\frac{dx_e}{dz} = \frac{1}{H(z)}[R_s(z) - I_s(z) - I_\chi(z)], \quad (1)$$

$$(1+z)\frac{dT_b}{dz} = \frac{8\sigma_T a_R T_{cmb}^4}{3m_e c H(z)} \frac{x_e}{1+f_{He}+x_e} (T_b - T_{cmb}) - \frac{2}{3k_B H(z)} \frac{K_\chi}{1+f_{He}+x_e} + 2T_b. \quad (2)$$

Here R_s is the standard recombination rate, I_s the ionization rate by standard sources, detailed discussion of these terms can be found in Ref. [18]. The extra ionization and heating terms due to dark matter annihilations are given by

$$I_\chi = \chi_i f \frac{\Gamma_{ann}}{n_b} \frac{2m_\chi c^2}{E_b}, \quad K_\chi = \chi_h f \frac{\Gamma_{ann}}{n_b} \frac{2m_\chi c^2}{E_b}; \quad (3)$$

where n_b is the baryon number per unit proper volume, and $E_b = 13.6$ eV is the ionization energy. A more detailed treatment would include helium, but as the spectrum of the injection energy is quite uncertain, we will not deal with these complications in this paper. Γ_{ann} is the annihilation rate. The factor f is a fudge factor denotes the fraction of the total energy which is deposited in the baryonic gas *in situ* (c.f. Ref. [18]), with $f_{max} = 1$. The absorbed energy contributes both to the ionization and heating of the gas. As a simple model for the division between these, we assume the respective fractions are given by [18]

$$\chi_i = (1 - x_e)/3, \quad \chi_h = (1 + 2x_e)/3 \quad (4)$$

where x_e is the fraction of free electrons. The annihilation rate of the dark matter is given by

$$\Gamma_{ann} = gn^2 \langle \sigma v \rangle = g \left(\frac{\rho_c}{m_\chi} \right)^2 \Omega_c^2 (1+z)^6 \langle \sigma v \rangle \quad (5)$$

where g is a degeneracy factor, n is the number density of the particle, and the angular brackets denote thermal average. The second equality applies in the case of homogeneous distribution. where ρ_c is the critical density

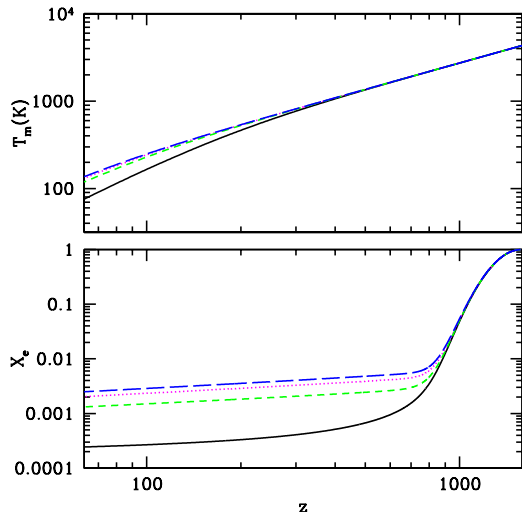


FIG. 1: The ionization fraction x_e and intergalactic medium temperature as a function of redshift z for model (a): the fiducial model which is the WMAP first year best fit Λ CDM model with no contribution from dark matter annihilation (black solid curve); for (b): $F_{26} = 1.0$ (green dotted curve); for (c): $F_{26} = 2.6$ (magenta dashed curve); and for (d): $F_{26} = 4.0$ (blue dotted - dashed curve). We only change F_{26} and keep other parameters fixed.

at $z = 0$, Ω_c is the relative density fraction of the dark matter. For Majorana particles (i.e. the particle and anti-particle are the same), $g = 1/2$. If the particles are not Majorana, we shall assume that the dark matter is made of equal numbers of particles and anti-particles, and $g = 1/4$. The effect of dark matter annihilation on the ionization is then entirely quantified by a parameter which characterizes the annihilation intensity:

$$F_{26} = 2gf \left(\frac{\langle \sigma v \rangle}{10^{-26} \text{cm}^3 \text{s}^{-1}} \right) \left(\frac{m_\chi c^2}{\text{GeV}} \right)^{-1}. \quad (6)$$

We modify the recombination code RECFAST [38] to take into account of these extra contributions. For details of such modification, see Ref.[18]. The recombination history for several different values of F_{26} parameter is shown in Fig. 1. As can be seen from the figure, with dark matter annihilations, the recombination process is slightly delayed and more extended. This is increasingly apparent for greater value of F_{26} . However, unlike the case of dark matter decay investigated in Ref. [18] where the ionization fraction could increase at lower redshift, the ionization fraction still decreases steadily to an asymptotic value at later time, because the annihilation rate drops as the number density of the dark matter particle drops with the expansion of the Universe. At the same time, the temperature of the gas is also slightly higher, but still decreases steadily, instead of raising drastically as in some decaying dark matter models.

The increase in free electron density may help to boost

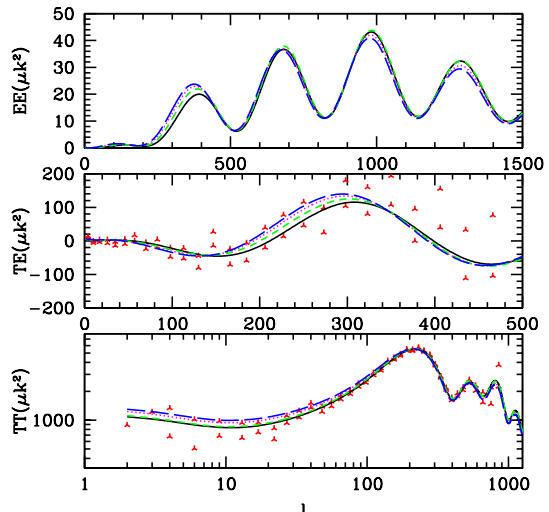


FIG. 2: The CMB angular power spectra for the models (a), (b), (c) (d) given in the previous figure, plotted along with the CMB data points with error bars used in our fit (for WMAP: first year data only).

the formation of molecule hydrogen, which is the most important coolant at the end of dark age. This might increase the formation rate of the first generation of stars. At the same time, the increase in gas temperature also raise the Jeans mass scale, and thus suppress star formation in smaller dark matter halos. The impact of dark matter annihilation on the formation of first generation of stars is therefore interesting and complicated, and we plan to investigate this problem in future works. With powerful 21cm interferometer arrays, it might be possible to have direct observations of gas temperature during the cosmic dark age [50, 51, 52, 53].

At present, however, the only available probe of this early epoch of the Universe is CMB anisotropy. The RECFAST code was used by the Boltzmann CMB code CAMB [36, 37] to calculate the recombination history. With the above modification, we can calculate the angular power spectra of CMB anisotropies. The spectra for the models described above are shown in Fig. 2. In the TT spectrum, the amplitudes at large scale (small l) are greater for the annihilation models. This is because, if all parameters are kept fixed, the spectrum at large l will be damped with a factor of $e^{-2\tau}$ where τ is the optical depth [10, 11], but when the spectrum is fitted to the data, the greater statistical weights at greater l will determine the normalization of the spectrum, so the lower l spectrum appears to be raised [18]. For the TE spectrum, both the position and height of the acoustic peaks are shifted, as one might expect for a model with delayed recombination history. The cross-correlations at small l do not increase much in our models, because at lower redshifts our models do not differ much from the standard. There are also variations in the EE power spectrum, particularly in the height of the peaks.

Over the past few years, the MCMC method has become a standard technique for exploring the multi-parameter space, obtaining estimates on the measurement error, and breaking the parameter degeneracies. The publicly available code package COSMOMC performs such calculation with the CAMB code as its driver for CMB calculation. We have adopted this package for our computation. We consider the following set of 7 cosmological parameters, $\Omega_b h^2, \Omega_c h^2, \theta, \tau, n_s, A_s, F_{26}$, where $\Omega_b h^2$ and $\Omega_c h^2$ are the physical density parameters for baryon and cold dark matter particle, θ is the ratio of the sound horizon at recombination to its angular diameter distance multiplied by 100, τ is the optical depth, n_s and A_s are the spectral index and amplitude of the primordial density perturbation power spectrum. We used the data from the WMAP [4, 5, 7, 8], ACBAR [41], Boomerang [42], CBI [43], and VSA [44] experiments in our analysis. After the release of the WMAP three year data [45, 46, 47, 48], we repeated our analysis with the new data.

III. RESULTS

In Fig. 3 we plot the marginalized probability distribution function (PDF) of the annihilation intensity parameter F_{26} and the mean relative likelihood. For the WMAP first year data, the PDF is fairly flat at $F \lesssim 1$, as the effect of dark matter annihilation on CMB is still too small compared with the measurement error at this point. The PDF drops more rapidly at $F_{26} > 1$, and falls below the 95% limit at $F_{26} \approx 2.6$. The mean relative likelihood function (dotted line) has a similar shape, although at $F_{26} < 1$ it falls more steadily. This shows that our result is robust. With the WMAP three year data, the peak of the PDF is still at $F_{26} = 0$, consistent with no detection, and the width of the PDF is much narrower, the %95 limit is at $F_{26} = 0.43$, and it dropping to 0 at $F_{26} \approx 0.6$. This indicates a significant increase in the precision and constraining power of the new data set, thanks in large part to the new EE power spectrum.

How does the addition of the dark matter annihilation intensity parameter F_{26} affects the global fitting of cosmological parameters? We list the best-fit values and errors of the cosmological parameters in Tab. I (WMAP first year) and Tab. II (WMAP three year). From the table, it seems that the mean value and errors of the other parameters are not significantly affected, as compared to the case of the standard Λ CDM model. We also plot the 2-d contours of the F_{26} parameter with other cosmological parameters in Fig. 4 (WMAP first year) and Fig. 5 (WMAP three year). With the WMAP first year data, we find that F correlates mainly with $n_s, \Omega_b h^2$ and A_s . One might naively expect a strong correlation of F_{26} with the reionization redshift z_{re} , and be surprised that this is not so. However, in the dark matter annihilation model described here, the impact on ionization fraction is strong at the very high redshifts of the epoch of re-

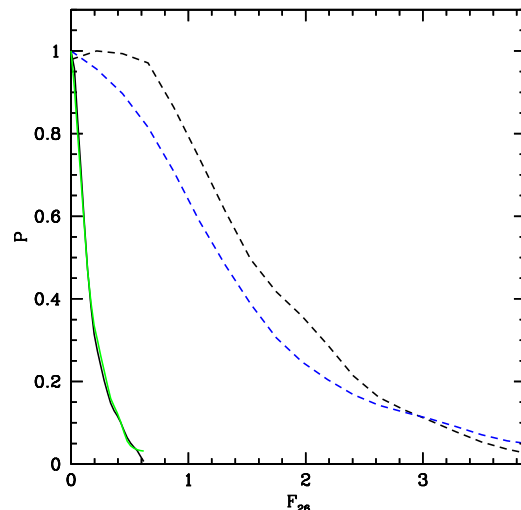


FIG. 3: The marginalized probability distribution function of the F_{26} parameter and the relative mean likelihood. The solid curves are for WMAP three year data, the dashed curves are for WMAP first year data. The normalization is such that the maximum of the function is 1.

combination, not at the lower redshifts of reionization. Indeed, we find that there is little variation in the low ℓ TE spectra for different values of the F parameter. With the WMAP three year data, which has EE power spectrum, the degeneracy is further reduced: there is very little correlation with any parameter.

The quality of the CMB data is going to be improved continuously. How is the F_{26} parameter going to be constrained with future data, e.g. those obtained with the Planck? To make forecasts on the measurement error, we use the Fisher matrix formalism (see e.g. Refs. [54, 55, 56, 57, 58]). The Fisher matrix is computed with

$$F_{ij} = \frac{\partial^2 \chi^2}{\partial \theta_i \partial \theta_j} \quad (7)$$

and

$$\chi^2 = \sum_X \sum_l \frac{(C_{X,l}^{obs} - C_{X,l}^{th})^2}{\sigma_{C_{X,l}}^2} \quad (8)$$

where $X = TT, TE, EE, BB$. In our calculation we assumed a sky coverage factor of 0.65, and we adopt a fiducial model which best fit the WMAP three year data. For the detector noise, we adopt the values given in Ref. [58] for the WMAP and Planck satellites. We have also calculated the Fisher matrix corresponding to three years of observation of the WMAP, and found that the result is in general agreement with that obtained with the MCMC method, as shown in the last column of Tab. I,II. There are some small residue differences. Given that we have also used data from several other experiments, and the error of the WMAP is more complicated than our simple

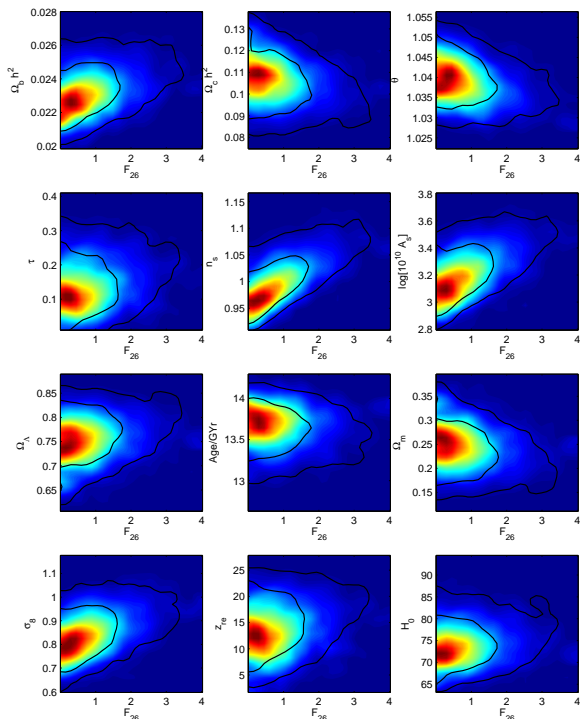


FIG. 4: The 2-D contours of the distribution of F and background parameters for WMAP first year data.

model with Gaussian beam, such differences are not unexpected. We conclude that the Fisher matrix estimation is basically reliable. The $1 - \sigma$ error on cosmological parameters calculated with the Fisher matrix formalism for one year Planck observation is given in Table. III. The expected error on the F_{26} parameter is 0.031.

The primary results of this paper is presented in Fig. 6, which is a synthesis of constraints on the light dark matter annihilation flux parameter F_{26} derived from the CMB as well as other methods. The three horizontal lines indicate %95 limits on F_{26} derived from CMB data. The upper two of these are derived from the analysis of the WMAP first year and three data, together with data from other current CMB experiments, using the MCMC method. The lowest one is our forecast on the potential limit derived from Planck one year observation using the Fisher matrix formalism. The impact of particle annihilation on CMB depends only on F_{26} , so these limits are independent of mass M .

The parameter space of the light dark matter is also constrained by other observations. In particular, the original motivation of the light dark matter is to explain the excess of positrons in the Galactic Center. The observed 0.511 MeV photon flux is $(1.05 \pm 0.06) \times 10^{-3} \text{ph cm}^{-2} \text{s}^{-1}$ with an extension of 8° [26]. The 0.511MeV photons are produced in the prompt annihilation of positron and the 2γ annihilation of positronium. For the positrons in the Galactic Center, observation indicates that the fraction of positronium formation is $f_p = 0.96$ [59], and the 2γ branching ratio of positro-

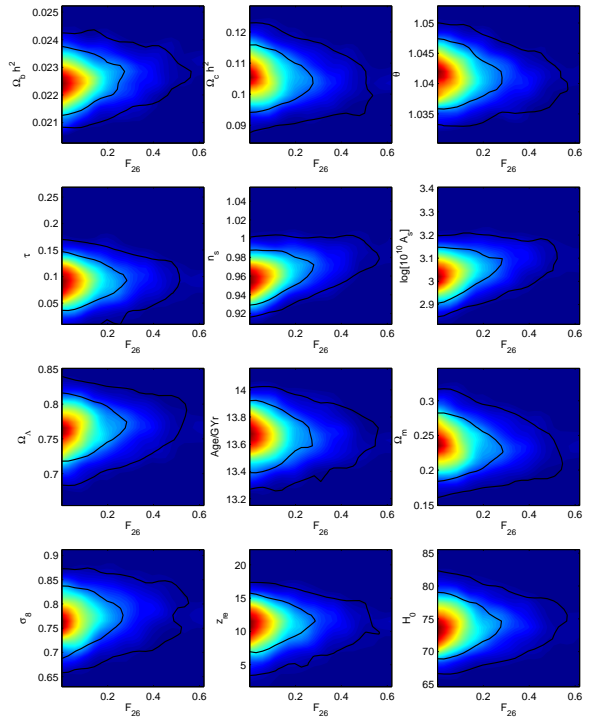


FIG. 5: The 2-D contours of the distribution of F and background parameters for WMAP three year data.

nium is 0.25, so for each positron the number of 0.511 MeV photon produced is $2p$ where $p = 1 - 0.75f_p$. The 0.511 MeV photon flux is then related to the dark matter annihilation cross section by

$$\Phi \cong 2pg\bar{J} \times 5.6 \left(\frac{\sigma v}{10^{-26} \text{cm}^3 \text{s}^{-1}} \right) \left(\frac{M}{\text{MeV}} \right)^{-2} \text{cm}^{-2} \text{s}^{-1} \text{sr}^{-1}, \quad (9)$$

where $\bar{J}(0.015 \text{sr}) = 231.8$ [60] for the Navarro-Frenk-White profile [61]. Thus, to produce the observed positrons by dark matter annihilation, the cross section of the dark matter is given by

$$\frac{\langle \sigma v \rangle}{10^{-26} \text{cm}^3 \text{s}^{-1}} = 7.8 \times 10^{-5} g^{-1} p^{-1} \left(\frac{M}{\text{MeV}} \right)^2. \quad (10)$$

In terms of F_{26} ,

$$F_{26} = 0.156 p^{-1} f \left(\frac{M}{\text{MeV}} \right). \quad (11)$$

Assuming $0.1 < f < 1$, we draw the favored region as the tilted band marked e^+e^- (raising from left to right). The band is bounded from left, as the mass of the dark matter particle must be greater than 0.511 MeV to produce electron-positron pair in its annihilation. By combining this requirement with the CMB bound on F_{26} , we can derive an upper bound on the dark matter particle mass. The uncertainty (width) of this e^+e^- band is mainly due to the uncertainty in f , hence the mass upper bound also depends on f . If we assume value $f \simeq 1$,

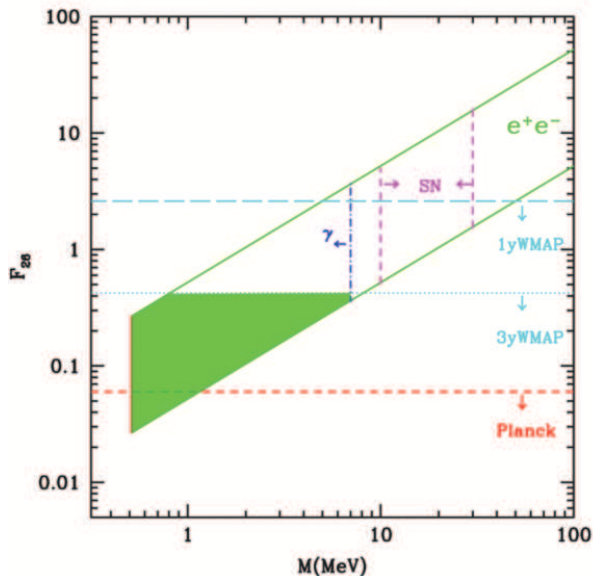


FIG. 6: The CMB constraint on the dark matter annihilation. The region between the two tilted lines are the region required for explain the positron excess in the Galactic Center. The lower and upper line corresponds to $f = 0.1$ and $f = 1$, respectively. The regions favored by Supernovae cooling/neutrino emission and continuum γ -ray flux are also marked.

i.e. a large part of the energy released during annihilation could contribute to the ionization process, which corresponds to the upper border of the e^+e^- band. In this case, even with the first year WMAP data, an upper bound of 5 MeV on the dark matter can be obtained. On the other hand, for small $f \sim 0.1$, the upper bound on the mass obtained with the WMAP first year data is about 50 MeV¹. With the WMAP three year data, the allowed region is further reduced. For $f = 1$, the upper bound on mass is only 0.8 MeV, which excludes most of the allowed mass range. Even for $f = 0.1$, we still obtain a strong limit of $M < 8\text{MeV}$. As we assume that the e^-e^+ pair is produced by dark matter annihilation (i.e. not invisible decay), it is unlikely for the value of f to be much smaller. This limit can be further improved with future high precision experiments such as the Planck Surveyor. The %95 limit for one year observation of Planck (assuming the same set of cosmological parameters) is $F_{26} \sim 0.06$. For $f = 1$, the whole mass range can be excluded. Even for $f = 0.1$, this will pro-

¹ These constraints are stronger than given in the first draft of this paper. In the first draft we assumed that all positrons annihilate in the two photon process. However, a large fraction of positrons would form positronium, and annihilate in three photon process, hence to produce the observed flux, greater annihilation rate is required. Also, in the first draft we made a mistake in converting units used in some literature to the units used in this paper.

duce an upper mass limit of about 1 MeV. The CMB limit can be evaded if one adopts a very small value of f . This would happen if, e.g., weakly interacting annihilation products such as neutrinos carry most of the energy away. Such annihilating dark matter would have little impact on baryonic gas, but could be constrained with neutrino detectors [62].

Beside the CMB and positron excess, the light dark matter can also be constrained with γ -ray emission from annihilation [63, 64, 65, 66], and from the cooling and neutrino emission of the core-collapse supernovae explosion [67]. The mass range of 10-30 MeV is favored by the SN argument, although this value can be lowered if the dark matter-neutrino interaction is not enhanced as expected. The limit derived from the γ -ray flux depends somewhat on the model and data adopted, ranging from 3 MeV [64] to 20 MeV [65]. On Fig. 6, we marked $M < 7.5$ MeV as derived from Ref. [66] as the γ limit. The favored regions derived with these methods do not overlap. The higher mass range favored by the supernova argument is also difficult to reconcile with the relic abundance of the dark matter, if it is produced by the conventional thermal mechanism. Our result based on the WMAP three year data is compatible with the γ -ray limits.

IV. CONCLUSION

We have investigated the effect of dark matter annihilation on recombination history and the CMB anisotropies. Because the annihilation rate is only significant at the high redshifts of the era of recombination, the shift in the CMB angular power spectra occurs mostly at high ℓ s, and the signature is distinct from that of an early reionization. The impact of the energy injection from annihilating dark matter on the ionization history and CMB spectra can be characterized by the annihilation intensity parameter, F_{26} (c.f. Eq. 6). The addition of this parameter does not significantly affect the uncertainty in the estimation of the other parameters. Using the currently available data, including WMAP first year and three data, as well as those from ACBAR, Boomerang, CBI and VAS, we obtained limits on this parameter. With the WMAP first year data, we can start to constrain the parameter space. Dark matter annihilation with $F_{26} > 2.6$ is excluded at %95 level, corresponding to mass greater than 60 MeV. The WMAP three year data, particularly the EE spectrum, provides much stronger constraint: $F_{26} < 0.43$ at %95 limit, corresponding to $M < 8$ MeV. This result is compatible with the limit derived from γ -ray observation [63, 64, 65, 66], and apparently excludes the region favored by the supernovae cooling argument [67]. With future CMB data such as those from Planck, these limits can be future strengthened, or even more interestingly, possible signal of dark matter annihilation could be discovered. In addition, heating of the baryonic gas to high temperature during the dark age

might be observable with future 21cm observations [53]. Discovery of such signal would provide strong evidence for energy injection from dark matter decay or annihilations.

Acknowledgments

We thank Bo Feng, Xiaojun Bi, Junqing Xia, Gongbo Zhao, Quan Guo, Yan Qu, Pengjie Zhang, Hongsheng

Zhao and John F. Beacom for discussions and suggestions. Our MCMC chain computation was performed on the Shenteng system of the Supercomputing Center of the Chinese Academy of Sciences. This work is supported by the National Science Foundation of China under the Distinguished Young Scholar Grant 10525314, the Key Project Grant 10533010, and Grant 10575004.

-
- [1] For a recent review, see e.g. G. Bertone, D. Hooper, and J. Silk, *Phys. Rep.* **405**, 279 (2005).
- [2] J. Miralda-Escude, *Science*, **300**, 1904(2003).
- [3] R. Barkana, and A. Loeb, *Phys. Rep.* **349**, 125 (2001).
- [4] C. L. Bennett et al., *Astrophys. J. Suppl. Ser.* **148**, 1 (2003).
- [5] G. Hinshaw et al., *Astrophys. J. Suppl. Ser.* **148**, 135 (2003)
- [6] D. N. Spergel et al., *Astrophys. J. Suppl. Ser.* **148**, 175 (2003).
- [7] A. Kogut et al., *Astrophys. J. Suppl. Ser.* **148**, 161 (2003).
- [8] L. Verde et al., *Astrophys. J. Suppl. Ser.* **148**, 195 (2003).
- [9] L. Page et al., *Astrophys. J. Suppl. Ser.* **148**, 233 (2003).
- [10] M. Zaldarriaga, *Phys. Rev. D* **55**, 1822 (1997).
- [11] M. Kaplinghat et al., *Astrophys. J.* **583**, 24 (2003).
- [12] G. P. Holder et al., *Astrophys. J.* **595**, 13 (2003).
- [13] M. Fukugita and M. Kawasaki, *Mon. Not. R. Astron. Soc.* **343**, L25 (2003).
- [14] R. Cen, *Astrophys. J. Lett.* **591**, L5 (2003).
- [15] N. Yoshida et al., *Astrophys. J.* **592**, 645 (2003).
- [16] A. Sokasian et al., *Mon. Not. R. Astron. Soc.* **344**, 607 (2003).
- [17] Z. Haiman and G. P. Holder, *Astrophys. J.* **595**, 1 (2003).
- [18] X. Chen and M. Kamionkowski, *Phys. Rev. D* **70**, 043502 (2004).
- [19] R. Bean, A. Melchiorri, and J. Silk, *Phys. Rev. D* **68**, 083501 (2003).
- [20] A. G. Doroshkevich et al, *Astrophys. J.* **586**, 709 (2003).
- [21] S. H. Hansen, Z. Haiman, *Astrophys. J.* **600**, 26 (2004).
- [22] E. Pierpaoli, *Phys. Rev. Lett.* **92**, 031301 (2004).
- [23] S. Kasuya, M. Kawasaki, N. Sugiyama, *Phys. Rev. D* **69**, 3512 (2004); S. Kasuya and F. Takahashi, *Phys. Rev. D* **70**, 103519 (2004).
- [24] N. Padmanabhan, D. P. Finkbeiner, *Phys. Rev. D* **72**, 023508 (2005).
- [25] G. Jungman, M. Kamionkowski, and K. Griest, *Phys. Rep.* **267**, 195 (1996).
- [26] J. Knodlseder et al., *Astron. Astrophys.* **441**, 513 (2005).
- [27] C. Boehm et al., *Phys. Rev. Lett.* **92**, 101301 (2004)
- [28] D. Hooper and L. Wang, *Phys. Rev. D* **70**, 063506 (2004).
- [29] S. Kasuya and F. Takahashi, *Phys. Rev. D* **72**, 085015 (2005); S. Kasuya and M. Kawasaki, *Phys. Rev. D* **73**, 063007 (2006).
- [30] K. M. Belotsky et al., *Grav. Cosmol.* **11**, 27 (2005) (e-print: astro-ph/0504621).
- [31] M. Mapelli, A. Ferrara, E. Pierpaoli, *Mon. Not. R. Astron. Soc.* **369**, 1719 (2006).
- [32] D. Gamerman, *Markov Chain Monte Carlo: Stochastic simulation for Bayesian inference*, Chapman and Hall (1997).
- [33] L. Knox, N. Christensen, and C. Skordis, *Astrophys. J. Lett.* **563**, L95 (2001).
- [34] A. Lewis and S. Bridle, *Phys. Rev. D* **66**, 103511 (2002).
- [35] <http://cosmologist.info/cosmomc>
- [36] A. Challinor, and A. Lasenby, *Astrophys. J.* **513**, 1 (1999); A. Lewis, A. Challinor, and A. Lasenby, *Astrophys. J.* **538**, 473 (2000).
- [37] <http://camb.info>
- [38] S. Seager, D. D. Sasselov, and D. Scott, *Astrophys. J. Lett.* **523**, L1 (1999).
- [39] The Planck Collaboration, Report-no: ESA-SCI(2005)1.
- [40] <http://www.rssd.esa.int/Planck>
- [41] C. L. Kuo et al. *Astrophys. J.* **600**, 32 (2004) .
- [42] T. E. Montroy et al., astro-ph/0507514.
- [43] T. J. Pearson et al. *Astrophys. J.* **591**, 556 (2003).
- [44] P. F. Scott et al. *Mon. Not. R. Astron. Soc.* **341**, 1076 (2003).
- [45] D. N. Spergel et al., astro-ph/0603449.
- [46] L. Page et al., astro-ph/0603450.
- [47] G. Hinshaw et al., astro-ph/0603451.
- [48] N. Jarosik et al., astro-ph/0603452.
- [49] <http://lambda.gsfc.nasa.gov/product/map/>
- [50] A. Loeb, and M. Zaldarriaga, *Phys. Rev. Lett.* **92**, (211301)2004.
- [51] R. Barkana, and A. Loeb, *Mon. Not. R. Astron. Soc.* **363**, L36 (2005).
- [52] S. Bharadwaj, S. S. Ali, *Mon. Not. R. Astron. Soc.* **352**, 142 (2004).
- [53] S. Furlanetto, S. P. Oh, E. Pierpaoli, astro-ph/0608385.
- [54] M. Tegmark, *Phys. Rev. D* **56**, 4514 (1997).
- [55] U. Seljak, *Astrophys. J.* **482**, 6 (1997).
- [56] M. Zaldarriaga and U. Seljak, *Phys. Rev. D* **55**, 1830 (1997).
- [57] M. Kamionkowski, A. Kosowsky, and A. Stebbins, *Phys. Rev. Lett.* **78**, (2058)1997.
- [58] D. J. Eisenstein, W. Hu, and M. Tegmark, *Astrophys. J.* **518**, 2 (1999).
- [59] P. Jean et al., *Astron. Astrophys.* **445**, 579 (2006).
- [60] Y. Ascasibar et al., *Mon. Not. R. Astron. Soc.* **368**, 1695 (2006).
- [61] J. F. Navarro, C. S. Frenk, S. D. M. White, *Astrophys. J.* **490**, 493 (1997).
- [62] J. F. Beacom, N. F. Bell, and G. D. Mack, astro-ph/0608090.

TABLE I: First year WMAP posterior constrains on cosmological parameters

Parameter	best-fit	mean	1 σ lower	1 σ upper	2 σ lower	2 σ upper	σ (fisher)
$100\Omega_b h^2$	2.226	2.411	2.244	2.586	2.129	2.872	0.072
$\Omega_c h^2$	0.109	0.105	0.0944	0.114	0.0850	0.127	0.0055
Θ_S	1.041	1.039	1.034	1.045	1.029	1.050	
τ	0.107	0.145	0.01	0.173	0.01	0.281	0.0185
F_{26}	0.267	0.94	0	1.13	0	2.62	0.317
n_s	0.97	1.006	0.962	1.050	0.937	1.106	0.026
$\log[10^{10} A_s]$	3.116	3.244	3.077	3.422	2.949	3.610	0.0796
Ω_Λ	0.745	0.766	0.723	0.810	0.663	0.845	
Age/Gyr	13.67	13.61	13.39	13.86	13.05	14.04	
Ω_m	0.255	0.234	0.190	0.277	0.155	0.337	
σ_8	0.82	0.855	0.766	0.945	0.700	1.046	
z_{re}	12.68	14.84	10.00	19.82	5.92	23.6	
H_0	72.1	74.57	70.26	78.99	66.56	84.95	0.0283

TABLE II: Three year WMAP data posterior constrains on cosmological parameters

Parameter	best-fit	mean	1 σ lower	1 σ upper	2 σ lower	2 σ upper	σ (fisher)
$100\Omega_b h^2$	2.249	2.257	2.192	2.325	2.128	2.394	0.054
$\Omega_c h^2$	0.1049	0.1047	0.099	0.111	0.092	0.118	0.0038
Θ_S	1.0411	1.0412	1.038	1.044	1.035	1.048	
τ	0.096	0.091	0.01	0.105	0.01	0.138	0.0116
F_{26}	0.007	0.147	0	0.174	0	0.424	0.173
n_s	0.956	0.964	0.947	0.981	0.932	0.999	0.0174
$\log[10^{10} A_s]$	3.033	3.049	2.983	3.113	2.917	3.178	0.043
Ω_Λ	0.767	0.766	0.738	0.794	0.704	0.820	
Age/Gyr	13.654	13.651	13.50	13.8	13.34	13.92	
Ω_m	0.2331	0.2336	0.206	0.261	0.179	0.295	
σ_8	0.764	0.771	0.729	0.812	0.689	0.851	
z_{re}	11.83	11.15	0.876	13.56	5.41	15.52	
H_0	73.95	74.11	71.28	76.91	68.62	80.40	0.0227

[63] J. F. Beacom, N. F. Bell, and G. Bertone Phys. Rev. Lett. **94**, 171301 (2005).

[64] J. F. Beacom and H. Yuksel, Phys. Rev. Lett. **97**, (071102)2006.

[65] K. Ahn and E. Komatsu ,Phys. Rev. D **72**, 061301 (2005).

[66] P. Sizun, M. Casse, and S. Schanne, Phys. Rev. D **74**, 063514 (2006).

[67] P. Fayet, D. Hooper and G. Sigl, Phys. Rev. Lett. **96**, 211302 (2006).

TABLE III: Fisher matrix forecast on the $1\text{-}\sigma$ error of cosmological parameters measured with the Planck satellite.

parameter	$\Omega_b h^2$	$\Omega_c h^2$	h	τ	A_s	n_s	F_{26}
error (1σ)	1.7×10^{-4}	1.5×10^{-3}	7.8×10^{-3}	0.0050	0.012	0.0042	0.031